of flowering-time gene SOC1 by CONSTANS and FLC via separate promoter motifs. *EMBO J.* **21,** 4327–4337 (2002).
25. Lee, H. *et al.* The AGAMOUS-LIKE 20 MADS domain protein integrates floral inductive pathways in *Arabidopsis*. *Genes Dev.* **14,** 2366–2376 (2000).
26. Koornneef, M., Hanhart, C., Van Loenen-Martinet, P. & Blankestijn-de Vries, H. The effect of daylength on the transition to flowering in phytochrome-deficient, late-flowering and double mutants of *Arabidopsis thaliana*. *Physiol. Plant* **95,** 260–266 (1995).
27. Blazquez, M. A., Trenor, M. & Weigel, D. Independent control of gibberellin biosynthesis and flowering time by the circadian clock in *Arabidopsis*. *Plant Physiol.* **130,** 1770–1775 (2002).

Supplementary Information accompanies the paper on **www.nature.com/nature**.

Acknowledgements We thank the Kasuza Research Institute and the *Arabidopsis* Stock Center for providing EST clone APZL03h11R and BAC F2J7, respectively; D. Weigel for providing *FT*- and *CO*-overexpressing lines, and for useful advice; P. Wigge, S. Mora-Garcia, D. Weigel, J. Nemhauser, M. Yanovsky and J. Casal for comments on the manuscript; L. Barden for figure preparation; and B. Smoot, N. Ga and M. Ledgerwood for technical assistance. This work was supported by a grant from the National Institutes of Health to J.C. (GM52413) and by the Howard Hughes Medical Institute. P.C. was a fellow of the PEW Latin American Fellows Program and Fundación Antorchas.

Competing interests statement The authors declare that they have no competing financial interests.

Correspondence and requests for materials should be addressed to J.C. (chory@salk.edu). The GenBank accession code for *PFT1* is AY170377.

CUL-4 ubiquitin ligase maintains genome stability by restraining DNA-replication licensing

Weiwei Zhong, Hui Feng, Fernando E. Santiago & Edward T. Kipreos

Department of Cellular Biology, University of Georgia, Athens, Georgia 30602, USA

To maintain genome stability, DNA replication is strictly regulated to occur only once per cell cycle. In eukaryotes, the presence of 'licensing proteins' at replication origins during the G1 cell-cycle phase allows the formation of the pre-replicative complex[1]. The removal of licensing proteins from chromatin during the S phase ensures that origins fire only once per cell cycle[1]. Here we show that the CUL-4 ubiquitin ligase temporally restricts DNA-replication licensing in *Caenorhabditis elegans*. Inactivation of CUL-4 causes massive DNA re-replication, producing cells with up to 100C DNA content. The *C. elegans* orthologue of the replication-licensing factor Cdt1 (refs 2, 3) is required for DNA replication. *C. elegans* CDT-1 is present in G1-phase nuclei but disappears as cells enter S phase. In cells lacking CUL-4, CDT-1 levels fail to decrease during S phase and instead remain constant in the re-replicating cells. Removal of one genomic copy of *cdt-1* suppresses the *cul-4* re-replication phenotype. We propose that CUL-4 prevents aberrant re-initiation of DNA replication, at least in part, by facilitating the degradation of CDT-1.

CUL-4 is a member of the cullin ubiquitin-ligase family[4]. Cullins function in cullin/RING finger complexes to catalyse the covalent attachment of ubiquitin to protein substrates to mark them for proteolysis[5]. In *C. elegans*, the *cul-4* gene is expressed throughout development. In adult hermaphrodites, *cul-4* messenger RNA is observed primarily in the germ line, with transient expression in the intestine of young adults (Fig. 1a, b; data not shown). *cul-4* maternal mRNA is present in early embryos and decreases during embryogenesis (Fig. 1c, d). In larvae, *cul-4* is broadly expressed, with high levels in proliferating tissues, notably in the intestine and germ line (Fig. 1e).

To probe *cul-4* function, we used RNA-mediated interference (RNAi)[6] to inactivate the *cul-4* gene. *cul-4* RNAi reduced *cul-4* mRNA to levels not significantly higher than background (Fig. 1f–h). The predominant *cul-4* RNAi phenotype was a developmental arrest at the L2 larval stage. We observed a pronounced increase in the size of blast cell nuclei in *cul-4* RNAi L2 larvae. In a *clr-1*(*e1745*) genetic background that allows the visualization of cell boundaries[7], *cul-4* RNAi produced a marked increase in the size of seam cells (Fig. 2a, b). However, the size of nuclei in the non-proliferative hyp7 syncytial cell[8] was unaffected by inactivation of *cul-4* (Fig. 2a, b). Larger cells were also observed among other *cul-4* RNAi blast cell lineages, including the M, Q, P and somatic gonad cell lineages (Fig. 2c–f; data not shown). Germ cells did not become enlarged. However, germ cells often entered meiosis prematurely to become sperm in the L2 larval stage; this is in contrast to the wild type, in which spermatogenesis occurs in the L4 larval stage[9] (Fig. 2e, f). We assume that this premature spermatogenesis results

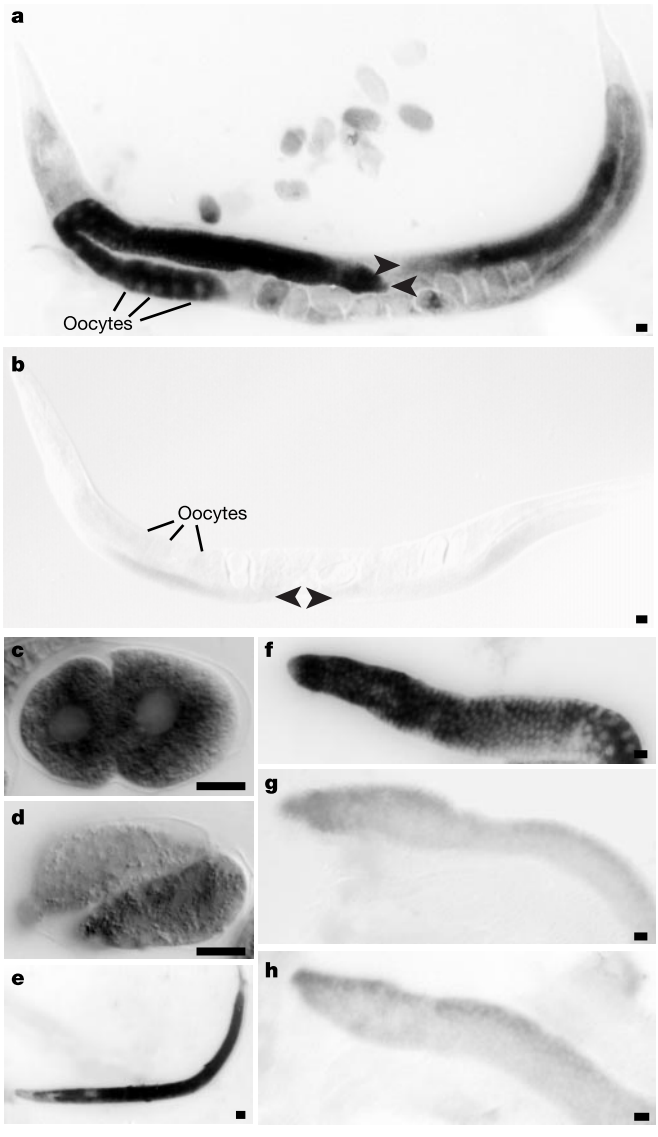

Figure 1 *cul-4* mRNA levels. **a**, **b**, *In situ* hybridization of wild-type adult hermaphrodites with *cul-4* antisense (**a**) or control sense (**b**) probes. Arrowheads mark the distal ends of the gonad arms; anterior oocytes are labelled. **c**–**e**, *In situ* hybridization with antisense *cul-4* probe of a two-cell-stage embryo (**c**), twofold-stage embryo (**d**) and L2 larva (**e**). **f**–**h**, *In situ* hybridization of dissected gonads from wild-type adult hermaphrodites (**f**, **h**) or wild-type hermaphrodite injected with *cul-4* dsRNA (**g**) probed with antisense *cul-4* (**f**, **g**) or sense *cul-4* (**h**). Scale bars, 10 μm.

from an inability of the somatic gonad lineage to produce distal tip cells (DTCs) that are required to prevent germ cells from entering meiosis[9].

We measured the amount of genomic DNA in enlarged *cul-4* RNAi blast cells and observed markedly elevated DNA levels. Two to three days post-hatch, *cul-4* RNAi seam cells contain up to 100C DNA content, compared with the 2C of the wild type (Figs 2g, h and 3d). Three distinct mechanisms can generate increased ploidy (Fig. 3a): (1) failed mitosis, in which a failure of chromosome separation and cytokinesis causes cells to enter G1 phase with a doubled DNA content[10]; (2) endoreplication, in which cells bypass mitosis and enter the next cell cycle with doubled DNA content[11]; and (3) re-replication due to origin re-firing, referred to here as 're-replication', in which cells remain in S phase and continuously re-initiate DNA replication[1].

These mechanisms can be distinguished by three criteria. First, the presence of mitotic entry distinguishes the failed mitosis mechanism from endoreplication and re-replication, neither of which entails mitosis (Fig. 3a). The percentage of mitotic cells was determined by immunodetection of the early mitotic marker phosphorylated histone H3 (ref. 12). In unsynchronized wild-type larvae, 3.8% of seam cells were mitotic (42/1116), whereas only 0.09% of *cul-4* RNAi seam cells were mitotic (1/1109), a 42-fold decrease (Fig. 3b). In addition, nuclear envelope breakdown (an early mitotic event) was not observed in the seam cell lineage of *cul-4* RNAi L1 larvae when followed by differential interference contrast (DIC) microscopy (0/3 larvae), but was readily apparent in wild-type L1 larvae (2/2). Therefore, the lack of mitotic entry precludes the failed mitosis mechanism.

Second, in both the failed mitosis and endoreplication mechanisms, cells do not arrest in S phase, but instead continue to cycle through G2 and G1 phases (Fig. 3a). The duration of S phase in

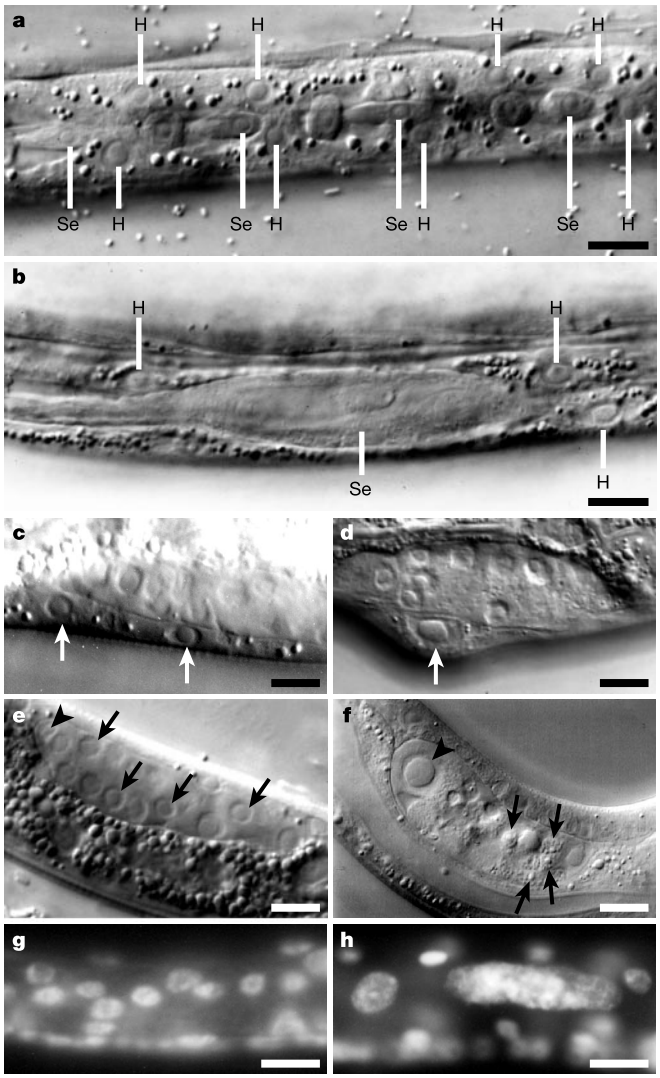

Figure 2 *cul-4* RNAi phenotype. **a**, **b**, DIC images of *clr-1*(*e1745*) (**a**) and *cul-4* RNAi, *clr-1*(*e1745*) (**b**) L2 larvae. Se, seam cell. H, hyp7 cell nuclei. **c**, **d**, DIC images of the ventral sides of wild-type (**c**) and *cul-4* RNAi (**d**) L2 larvae; arrows indicate P cells. **e**, **f**, Germ line of wild-type (**e**) and *cul-4* RNAi (**f**) L2 larvae. Arrowheads indicate DTC (**e**) or enlarged somatic gonad cell (**f**). Arrows indicate mitotic germ cells (**e**) or sperm (**f**). **g**, **h**, PI stain of genomic DNA in wild-type (**g**) and *cul-4* RNAi (**h**) L2 larvae. Scale bars, 10 μm.

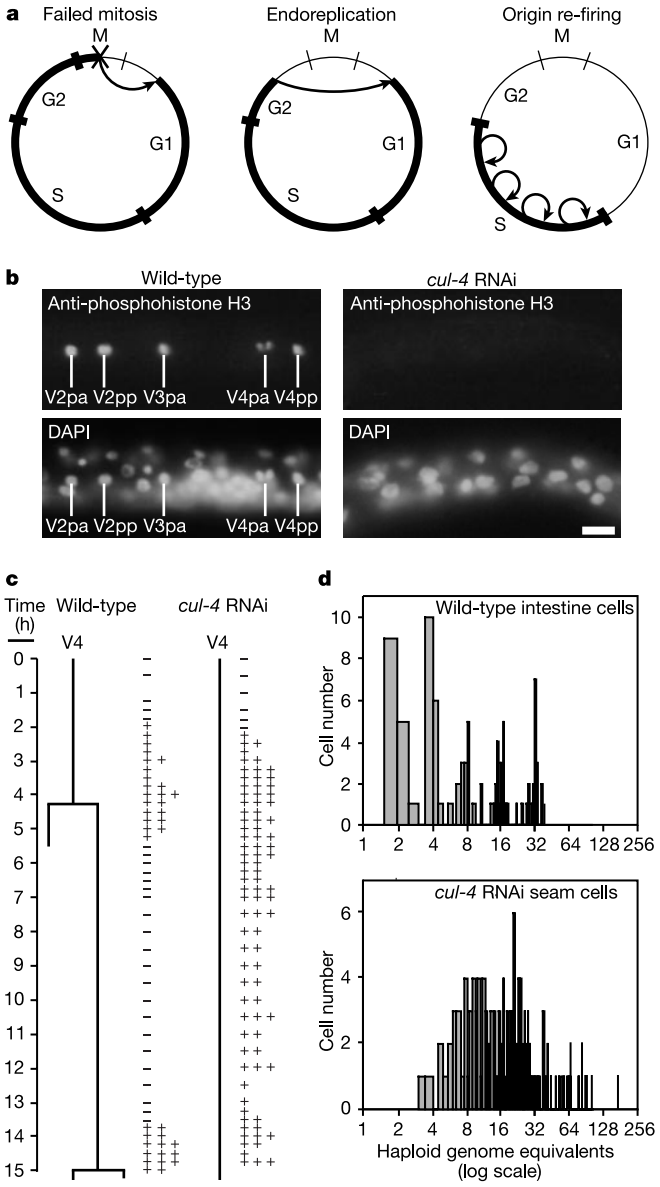

Figure 3 DNA re-replication in *cul-4* RNAi seam cells. **a**, Three mechanisms that generate increased ploidy. Dark lines represent the cell-cycle pathways. **b**, Anti-phosphorylated histone H3 and DAPI stain of wild-type and *cul-4* RNAi L2 larvae. Wild-type seam cells are named. Scale bar, 10 μm. **c**, L1 lineage and rnr::GFP expression pattern of the V4 seam cell in wild-type and *cul-4* RNAi larvae. Minus symbols denote no GFP fluorescence. Plus symbols indicate the intensity of rnr::GFP fluorescence. **d**, Histogram of DNA content of intestine cells from unsynchronized wild-type larvae (top) and seam cells from unsynchronized *cul-4* RNAi larvae (bottom).

seam cells was measured using a reporter construct in which the S-phase-specific ribonucleotide reductase (rnr) promoter drives green fluorescent protein (GFP) expression[13]. We found that rnr::GFP expression began in both wild-type and *cul-4* RNAi seam cells at 2 h post-hatch (Fig. 3c). The wild-type rnr::GFP signal ended at approximately 5 h post-hatch, and did not resume until 14 h post-hatch, before the next cell division. By contrast, *cul-4* RNAi seam cells expressed rnr::GFP continuously through 15 h post-hatch (Fig. 3c). To further confirm that *cul-4* RNAi seam cells were in S phase during the period between wild-type mitotic divisions, we tested for incorporation of the thymidine analogue 5-bromodeoxyuridine (BrdU) into genomic DNA during a window of 5–11 h post-hatch. Wild-type seam cells did not incorporate BrdU during this time period (0/50); by contrast, 87.5% of *cul-4* RNAi seam cells incorporated BrdU (42/48). These results indicate that *cul-4* RNAi cells undergo an S-phase arrest, thereby supporting the re-replication model and arguing against the other two models.

Finally, in the failed mitosis and endoreplication mechanisms, increases in ploidy occur through doublings of genomic DNA, whereas in the re-replication mechanism ploidy increases are not quantized (Fig. 3a). The DNA content of *cul-4* RNAi seam cells was measured and found to increase continuously, rather than in doublings of 2C, as occurs in wild-type intestine cells that undergo endoreplication at each larval moult[14] (Fig. 3d). Taken together, these data suggest that the markedly increased ploidy in *cul-4* RNAi cells results from DNA re-replication.

The re-replication phenotype suggested a defect in DNA-replication licensing, which limits the extent of DNA replication in S phase[1]. Cdt1 is a key replication-licensing factor in both yeast and metazoa[2,3,15,16]. We identified a single *C. elegans* Cdt1 orthologue, *cdt-1*. In pairwise alignments, CDT-1 has 23%, 20%, 19% and 17% identity with its *Homo sapiens*, *Drosophila melanogaster*, *Schizosaccharomyces pombe* and *Saccharomyces cerevisiae* orthologues[2,15,17,18], respectively. CDT-1 is required for DNA replication in *C. elegans*. *cdt-1* RNAi embryos arrest with approximately 60 cells and contain only trace amounts of DNA, indicating a virtually complete cessation of DNA replication, although early cell divisions occur (Fig. 4a). Unequal DNA segregation and DNA bridges between dividing cells are observed during these early cell divisions, presumably secondary consequences of the defective DNA replication (Fig. 4b).

We generated affinity-purified anti-CDT-1 antibody, which recognizes a single band of approximately the predicted size of 84.5 kDa on a western blot (Fig. 4c). Immunofluorescence with this antibody was used to determine the CDT-1 expression pattern. In adults, CDT-1 is present in germ cell nuclei and is enriched in oocyte nuclei (data not shown). In early embryos, CDT-1 is localized to chromosomes in mitotic cells during anaphase and early telophase (Fig. 4b; data not shown). CDT-1 nuclear staining is not present in S phase, which directly follows mitosis in the early embryo[19] (Fig. 4b).

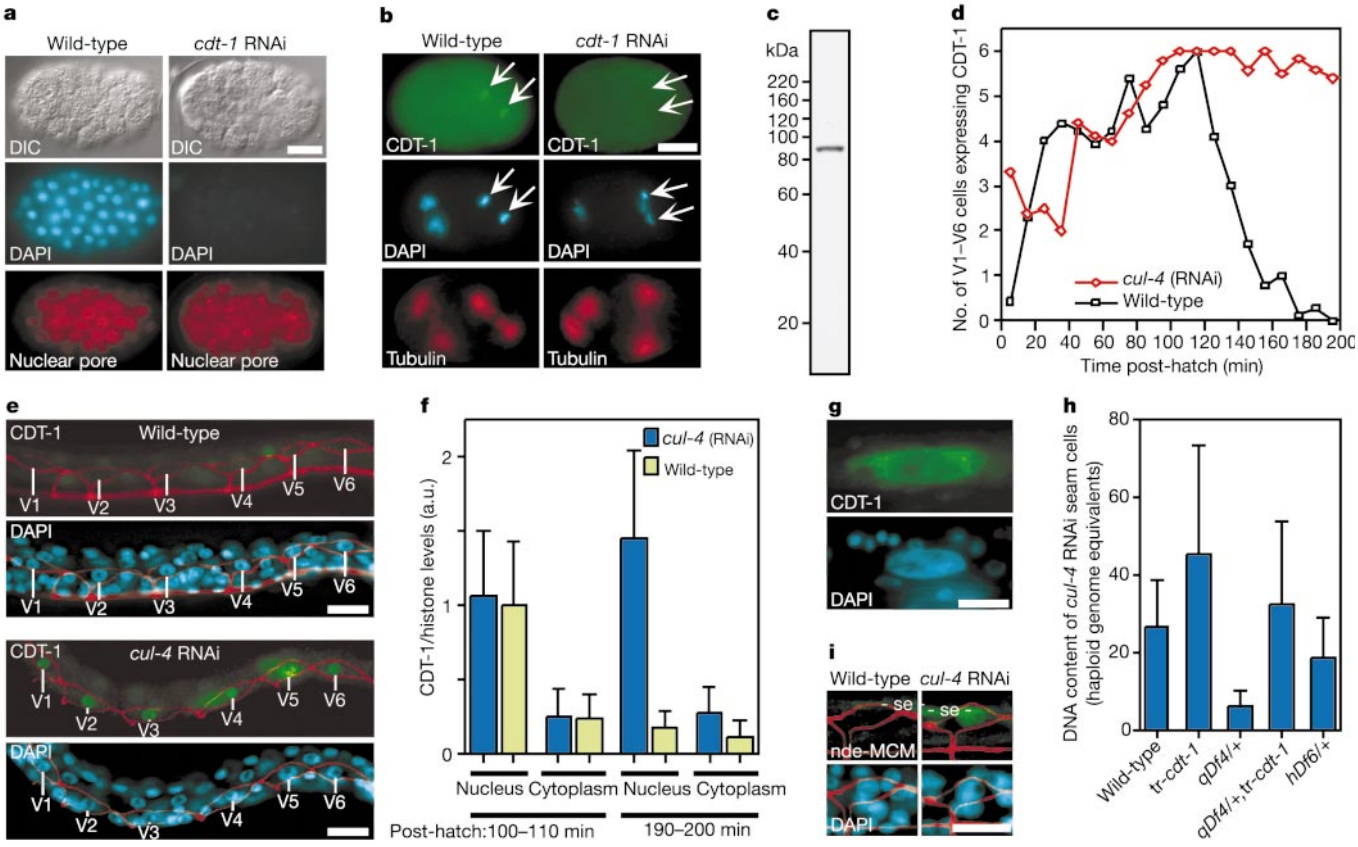

Figure 4 CDT-1 expression in *cul-4* RNAi animals. **a**, DIC, DAPI and anti-nuclear pore stain of 60-cell-stage wild-type and arrested *cdt-1* RNAi embryos. **b**, Anti-CDT1, DAPI and anti-α-tubulin stain of two-cell stage wild-type and *cdt-1* RNAi embryos. The *cdt-1* RNAi DAPI exposure is twice that of the wild type. Arrows indicate anaphase chromosomes. **c**, Anti-CDT-1 western blot of wild-type lysate. **d**, The average number of V1–V6 seam cells with nuclear CDT-1 in wild-type (squares) and *cul-4* RNAi (diamonds) animals at times post-hatch. **e**, Wild-type and *cul-4* RNAi larvae at 200 min post-hatch, stained with anti-CDT-1, DAPI and anti-AJM-1 (ref. 28) (red overlay, highlighting seam cell boundaries). **f**, Anti-CDT-1 levels in V1–V6 seam cell nuclei and cytoplasm relative to anti-histone (a permeabilization control) in wild-type (green) and *cul-4* RNAi (blue) larvae at the times indicated. **g**, Anti-CDT-1 and DAPI stain of enlarged *cul-4* RNAi seam cell. **h**, DNA content of seam cells upon *cul-4* RNAi in the strains listed ('tr-*cdt-1*' denotes a strain expressing transgenic *cdt-1*). **i**, Non-detergent-extractable anti-MCM and DAPI stain of wild-type and *cul-4* RNAi seam cells at 225 min post-hatch, with anti-AJM-1 overlaid (red). Non-specific anti-MCM staining of the hypodermal seam ridge is marked (-se-). Scale bars, 10 μm.

Anti-CDT-1 staining in embryos is abolished by *cdt-1* RNAi, indicating the validity of the staining pattern (Fig. 4b).

Newly hatched larvae lack detectable CDT-1 expression. However, CDT-1 levels are transiently increased in the nuclei of blast cells before their mitotic divisions. We examined the timing of CDT-1 expression in the first cell divisions of the V1–V6 seam cells, which enter S phase at 2 h post-hatch (see Fig. 3c for timing). In the wild type, CDT-1 expression began approximately 20 min after hatching in a subset of seam cells, and by 120 min post-hatch all seam cells expressed CDT-1 at high levels (Fig. 4d, f). At 130 min post-hatch, the number of seam cells with CDT-1 protein dropped precipitously, and by 150 min post-hatch most seam cells no longer had CDT-1 protein (Fig. 4d–f). Significantly, the decrease in CDT-1 levels in S-phase cells occurred in both the nucleus and cytoplasm ($P < 1 \times 10^{-10}$ and $P < 0.0005$, respectively), indicating that CDT-1 does not undergo subcellular redistribution, but instead is degraded (Fig. 4f). A similar rapid disappearance of Cdt1 in S-phase cells is observed in fission yeast and mammalian cells, and in the latter the degradation of Cdt1 has been shown to occur through the ubiquitin proteolytic pathway; however, the ubiquitin ligase involved remains unknown[2,20].

In *cul-4* RNAi animals, there was faint CDT-1 expression in some seam cells at hatch, but this expression increased with a time course similar to that in wild-type animals, so that at 120 min post-hatch all seam cells expressed CDT-1 with a staining intensity similar to that of wild-type cells (Fig. 4d, f). However, in marked contrast to wild type, CDT-1 levels did not drop after 120 min post-hatch, remaining at elevated levels through the S phase (Fig. 4d–f). In 2-day-old arrested *cul-4* RNAi larvae, approximately half of the enlarged cells were actively synthesizing DNA, as shown by the incorporation of BrdU, and of these cells, 98% (97/99) had CDT-1 protein, further demonstrating that CDT-1 is present in S-phase *cul-4* RNAi cells. The CDT-1 protein in re-replicating cells is generally nuclear, but can also be present in both the nucleus and cytoplasm (Fig. 4g). These results indicate that CUL-4 is required for the rapid decrease of CDT-1 levels in S-phase cells.

If a failure to eliminate CDT-1 from S-phase cells were contributing to the *cul-4* RNAi re-replication phenotype, then overexpression of CDT-1 would be expected to enhance the phenotype, and conversely, removal of one copy of the *cdt-1* gene might reduce the level of CDT-1 sufficiently to suppress the phenotype. Attempts to overexpress *cdt-1* using microinjection to introduce transgenic *cdt-1* expressed from its own promoter or the heatshock *hsp16-2* promoter failed due to lethality among the F1 progeny (data not shown). Subsequently, microparticle bombardment, which produces chromosomal integrations of single or few copies[21], was used to create a viable strain carrying transgenic *cdt-1* expressed from its own promoter. While *cul-4* RNAi produced seam cells with an average of 27C DNA content in wild-type larvae 2 days post-hatch, *cul-4* RNAi in the *cdt-1* overexpression strain produced an average of 45C DNA content, indicating a significant enhancement of the re-replication phenotype ($P < 0.05$) (Fig. 4h).

We tested for suppression of the *cul-4* RNAi phenotype by analysing the extent of re-replication in a strain heterozygous for the *qDf4* deficiency, which removes the *cdt-1* gene. Strikingly, the *cul-4* RNAi re-replication phenotype was suppressed fivefold in this strain ($P < 1 \times 10^{-6}$) (Fig. 4h). Reintroduction of the *cdt-1* gene into the *qDf4* heterozygous strain abolished the suppression, indicating that this was due to the loss of one copy of the *cdt-1* gene (Fig. 4h). By contrast, there was no significant suppression of the *cul-4* RNAi re-replication phenotype in a strain heterozygous for the *hDf6* deficiency, which deletes the orthologue of the replication-licensing factor Cdc6 (Fig. 4h).

In yeast and vertebrates, Cdt1 functions to license DNA for replication by promoting the binding of the Mcm2-7 putative replication helicase complex to replication origins to form the pre-replicative complex[1]. In vertebrates, Mcm2-7 remains localized to the nucleus after DNA replication, but dissociates from chromatin and can be extracted from nuclei with detergent[22]. Therefore, the presence of non-detergent extractable Mcm2-7 (nde-MCM) is an indication that chromatin has been licensed for replication. In early *C. elegans* embryos, all nuclei stain positive with an antibody that recognizes a conserved region of the MCM2-7 proteins. However, on detergent extraction, anti-MCM2-7 staining is only observed in telophase nuclei and smaller S-phase nuclei, consistent with MCM2-7 removal from replicated chromatin (data not shown). In larvae, nde-MCM is present in seam cell nuclei with a time course that is slightly delayed relative to nuclear CDT-1. At 120–135 min post-hatch, 95% of wild-type and 92% of *cul-4* RNAi seam cells had nde-MCM ($n = 84$ and 78, respectively). Wild-type seam cells lost nde-MCM after S phase, with only 6% positive for nde-MCM at 225–240 min post-hatch ($n = 102$). By contrast, 81% of *cul-4* RNAi seam cells had nde-MCM at 225–240 min post-hatch ($n = 120$) (Fig. 4i). These results indicate that MCM2-7 remains associated with chromatin in re-replicating *cul-4* RNAi seam cells. Taken together, our results suggest that CUL-4 maintains genome stability by removing CDT-1 from S-phase cells, which ensures that CDT-1 is not available to reload MCM2-7 onto chromatin to re-initiate replication origin firing.

In the early embryonic cell divisions of *Xenopus*, Cdt1 is regulated by association with the inhibitory protein Geminin[18,23]. Our observations indicate that the degradation of CDT-1 during S phase is crucial for the prevention of DNA re-replication, and they suggest that other CDT-1 control pathways, if present, cannot compensate for a failure of this central regulatory mechanism. In other eukaryotes, redundant controls operate to restrain DNA-replication licensing[1]. In yeast, disruption of multiple controls is required to produce substantial re-replication[24,25]. That inactivation of only a single gene, *cul-4*, leads to massive re-replication implies that CUL-4 is likely to regulate multiple aspects of DNA-replication licensing. □

Methods

Genetics and RNAi

The following strains of *C. elegans* were used: N2, wild type; CB3241 (*clr-1*(*e1745*)), VT765 (*unc-36*(*e251*), *maIs*103 (*unc-36*(+), rnr::GFP)); KR926 (*hDf6*, *dpy-5*(*e61*), *unc-13*(*e450*)/*szT1*, *unc-3*(*e151*)/*szT1*); JR667 (*unc-119*(*e2498*::Tc1), *wIs51* (*unc-119*(+), seam cell GFP marker)); ET117 (*unc-119*(*ed3*), *ekIs1* (pID2.02/*cdt-1*)); ET121 (*qDf4*/*unc-11*(*e47*)); and ET122 (*qDf4*/*unc-11*(*e47*), *ekIs1* (pID2.02/*cdt-1*)). The following strains were used in Fig. 4h: N2; ET117; ET121; ET122; and KR926. The strains heterozygous for deficiencies *qDf4* and *hDf6* appear to be wild type, with normal DNA levels (data not shown). Plasmid pID2.02/*cdt-1* was created by cloning genomic *cdt-1*, including 727 base pairs upstream of the translational start (Y54E10A sequences 69,104–63,789, GenBank accession number AC024810), into plasmid pID2.02, which contains genomic *unc-119* sequence. pID2.02/*cdt-1* was introduced into *unc-119*(*ed3*) homozygotes by microparticle bombardment as described[21]. RNAi was performed using double-stranded RNA (dsRNA) derived from complementary DNA clones for *cul-4* (yk34c8, GenBank accession number D36543) and *cdt-1*/Y54E10A.15 (yk10c5, GenBank accession number D34651). RNA was synthesized with Ambion T3 and T7 MegaScript kits. dsRNA was annealed and injected at a concentration of 0.5–1 mg ml^{-1} into L4 larvae or young adults as described[6], and progeny were analysed. Similar phenotypes were also obtained with the RNAi feeding method[26].

Antibodies and immunodetection

The *C. elegans cdt-1* and *cdc-6* genes were identified using BLAST[27] searches of National Center for Biotechnology Information databases for homologues of yeast and human Cdt1 and Cdc6. Anti-CDT-1 sera were produced in rabbits using purified recombinant His-tagged full-length CDT-1 fusion protein expressed from the pET15b vector (Novagen). Affinity purification was performed with His-CDT-1 fusion protein linked to activated CL4B Fast flow Sepharose (Amersham). Affinity-purified anti-CDT-1 antibodies from two different rabbits gave the same pattern of immunofluorescence staining. Other antibodies used were directed against: α-tubulin (N356, Amersham); nuclear pore (Mab414, BabCo); the adhesion junction component AJM-1 (ref. 28) (MH27, Developmental Studies Hybridoma Bank); BrdU (Sigma); phosphorylated histone H3 (Upstate Biotechnology); histone (Chemicon International); and pan-MCM (BD Pharmingen). Secondary antibodies were anti-rabbit and anti-mouse Alexa Fluor 488, 546 and 633 (Molecular Probes). Western blot with anti-CDT-1 antibody was performed with mixed-stage wild-type lysate separated on a NuPAGE 4–12% acrylamide gel (Invitrogen) and visualized by chemiluminescence using the SuperSignal West Femto substrate (Pierce). Immunofluorescence was performed on animals fixed using the 'freeze–crack' method as described[29]. DNA was stained with either 1 μg ml^{-1} 4,6-diamidino-2-

phenylindole (DAPI) or with 50 μg ml^{-1} propidium iodide (PI) after 20 μg ml^{-1} RNase A treatment for 1 h at 37 °C. For analysis of CDT-1 expression in larvae at set times after hatching, pretzel-stage embryos were collected, and at 10-min intervals hatched larvae were transferred to plates with OP50 bacteria. An average of 9.4 larvae (range, 5–27) were analysed for each time point. In the anti-CDT-1 images of Fig. 4e, out-of-focus light near the seam cells derives from CDT-1-positive intestine cells located below the seam cells. For detergent extraction of MCM proteins, slides were freeze-fractured, incubated for 5 min in a 4 °C solution of 10 mM HEPES-KOH, pH 7.4, 300 mM sucrose, 100 mM NaCl, 3 mM $MgCl_2$, 0.5% Triton X-100 and protease inhibitor cocktail (Roche), then processed for immunofluorescence according to the freeze–crack protocol[29].

In situ hybridization

Antisense and sense digoxigenin-labelled RNA probes were created from full-length *cul-4* cDNA using Ambion MegaScript T7 and T3 kits with digoxigenin-11-UTP (Roche). *In situ* hybridization was performed on whole animals, embryos or gonad arms dissected from hermaphrodites 2 days post-injection as described[30]. Quantification of *cul-4 in situ* hybridization levels in dissected gonads revealed: 100 ± 23 arbitrary units (a.u.) for wild-type antisense; 11 ± 28 a.u. for *cul-4* RNAi antisense; and 0 ± 16 a.u. for wild-type sense, $n = 10$ for each.

Microscopy

Animals were observed by DIC and immunofluorescence microscopy using a Zeiss Axioskop microscope. Images were taken with either TechPan film (Kodak) or a Hamamatsu ORCA-ER digital camera with Openlab 3.0.8 software (Improvision). Images were processed with Adobe Photoshop 6.0. Matched images were taken with the same exposure and processed identically. Matched images of anti-CDT-1, anti-AJM-1 and DAPI for Fig. 4e were deconvolved to equivalent extents using multineighbour deconvolution (Openlab). For quantification of GFP expression, generally two to three animals were observed per time point and the signals were averaged. Note that rnr::GFP signal persists beyond S phase in wild-type cells because of the perdurance of GFP protein. DNA was quantified from serial confocal images of PI-stained cells as described[30]. For the seam cell DNA quantification in Fig. 4h, $n = 15$ for each strain. Anti-CDT-1 and anti-histone staining (Fig. 4f) were quantified from confocal images; $n = 33$, 19, 8 and 39 for wild-type 100–110 min, wild-type 190–200 min, *cul-4* RNAi 100–110 min, and *cul-4* RNAi 190–200 min post-hatch, respectively. Means are presented with standard deviations. Statistical significance was determined with Student's *t*-test (two-tailed, equal variance).

Received 5 February; accepted 8 April 2003; doi:10.1038/nature01747.

1. Blow, J. J. & Hodgson, B. Replication licensing—defining the proliferative state? *Trends Cell Biol.* **12,** 72–78 (2002).
2. Nishitani, H., Lygerou, Z., Nishimoto, T. & Nurse, P. The Cdt1 protein is required to license DNA for replication in fission yeast. *Nature* **404,** 625–628 (2000).
3. Maiorano, D., Moreau, J. & Mechali, M. XCDT1 is required for the assembly of pre-replicative complexes in *Xenopus laevis*. *Nature* **404,** 622–625 (2000).
4. Nayak, S. *et al.* The *Caenorhabditis elegans* Skp1-related gene family: diverse functions in cell proliferation, morphogenesis, and meiosis. *Curr. Biol.* **12,** 277–287 (2002).
5. Tyers, M. & Jorgensen, P. Proteolysis and the cell cycle: with this RING I do thee destroy. *Curr. Opin. Genet. Dev.* **10,** 54–64 (2000).
6. Fire, A. *et al.* Potent and specific genetic interference by double-stranded RNA in *Caenorhabditis elegans*. *Nature* **391,** 806–811 (1998).
7. Hedgecock, E. M., Culotti, J. G. & Hall, D. H. The *unc-5*, *unc-6*, and *unc-40* genes guide circumferential migrations of pioneer axons and mesodermal cells on the epidermis in *C. elegans*. *Neuron* **4,** 61–85 (1990).
8. Sulston, J. E. & Horvitz, H. R. Post-embryonic cell lineages of the nematode, *Caenorhabditis elegans*. *Dev. Biol.* **56,** 110–156 (1977).
9. Seydoux, G. & Schedl, T. The germline in *C. elegans*: origins, proliferation, and silencing. *Int. Rev. Cytol.* **203,** 139–185 (2001).
10. Lorson, M. A., Horvitz, H. R. & van den Heuvel, S. LIN-5 is a novel component of the spindle apparatus required for chromosome segregation and cleavage plane specification in *Caenorhabditis elegans*. *J. Cell Biol.* **148,** 73–86 (2000).
11. Edgar, B. A. & Orr-Weaver, T. L. Endoreplication cell cycles: more for less. *Cell* **105,** 297–306 (2001).
12. Hendzel, M. J. *et al.* Mitosis-specific phosphorylation of histone H3 initiates primarily within pericentromeric heterochromatin during G2 and spreads in an ordered fashion coincident with mitotic chromosome condensation. *Chromosoma* **106,** 348–360 (1997).
13. Hong, Y., Roy, R. & Ambros, V. Developmental regulation of a cyclin-dependent kinase inhibitor controls postembryonic cell cycle progression in *Caenorhabditis elegans*. *Development* **125,** 3585–3597 (1998).
14. Hedgecock, E. M. & White, J. G. Polyploid tissues in the nematode *Caenorhabditis elegans*. *Dev. Biol.* **107,** 128–133 (1985).
15. Whittaker, A. J., Royzman, I. & Orr-Weaver, T. L. *Drosophila* double parked: a conserved, essential replication protein that colocalizes with the origin recognition complex and links DNA replication with mitosis and the down-regulation of S phase transcripts. *Genes Dev.* **14,** 1765–1776 (2000).
16. Cimbora, D. M. & Groudine, M. The control of mammalian DNA replication: a brief history of space and timing. *Cell* **104,** 643–646 (2001).
17. Tanaka, S. & Diffley, J. F. Interdependent nuclear accumulation of budding yeast Cdt1 and Mcm2-7 during G1 phase. *Nature Cell Biol.* **4,** 198–207 (2002).
18. Wohlschlegel, J. A. *et al.* Inhibition of eukaryotic DNA replication by Geminin binding to Cdt1. *Science* **290,** 2309–2312 (2000).
19. Edgar, L. G. & McGhee, J. D. DNA synthesis and the control of embryonic gene expression in *C. elegans*. *Cell* **53,** 589–599 (1988).
20. Nishitani, H., Taraviras, S., Lygerou, Z. & Nishimoto, T. The human licensing factor for DNA replication Cdt1 accumulates in G1 and is destabilized after initiation of S-phase. *J. Biol. Chem.* **276,** 44905–44911 (2001).
21. Praitis, V., Casey, E., Collar, D. & Austin, J. Creation of low-copy integrated transgenic lines in *Caenorhabditis elegans*. *Genetics* **157,** 1217–1226 (2001).
22. Todorov, I. T., Attaran, A. & Kearsey, S. E. BM28, a human member of the MCM2-3-5 family, is displaced from chromatin during DNA replication. *J. Cell Biol.* **129,** 1433–1445 (1995).
23. Tada, S., Li, A., Maiorano, D., Mechali, M. & Blow, J. J. Repression of origin assembly in metaphase depends on inhibition of RLF-B/Cdt1 by geminin. *Nature Cell Biol.* **3,** 107–113 (2001).
24. Nguyen, V. Q., Co, C. & Li, J. J. Cyclin-dependent kinases prevent DNA re-replication through multiple mechanisms. *Nature* **411,** 1068–1073 (2001).
25. Yanow, S. K., Lygerou, Z. & Nurse, P. Expression of Cdc18/Cdc6 and Cdt1 during G2 phase induces initiation of DNA replication. *EMBO J.* **20,** 4648–4656 (2001).
26. Timmons, L. & Fire, A. Specific interference by ingested dsRNA. *Nature* **395,** 854 (1998).
27. Altschul, S. F. *et al.* Gapped BLAST and PSI-BLAST: a new generation of protein database search programs. *Nucleic Acids Res.* **25,** 3389–3402 (1997).
28. Koppen, M. *et al.* Cooperative regulation of AJM-1 controls junctional integrity in *Caenorhabditis elegans* epithelia. *Nature Cell Biol.* **3,** 983–991 (2001).
29. Miller, D. M. & Shakes, D. C. in *Caenorhabditis elegans: Modern Biological Analysis of an Organism* (eds Epstein, H. F. & Shakes, D. C.) 365–394 (Academic Press, San Diego, 1995).
30. Feng, H. *et al.* CUL-2 is required for the G1-to-S phase transition and mitotic chromosome condensation in *Caenorhabditis elegans*. *Nature Cell Biol.* **1,** 486–492 (1999).

Acknowledgements We thank Y. Kohara, A. Fire, G. Seydoux, R. Roy and V. Ambros for reagents; the *Caenorhabditis* Genetics Center for nematode strains; R. Santurri for technical help; and H. Cai and P. Shen for critical reading of the manuscript. This work was supported by a grant from the National Institutes of Health to E.T.K.

Competing interests statement The authors declare that they have no competing financial interests.

Correspondence and requests for materials should be addressed to E.T.K. (ekipreos@cb.uga.edu).

RecBCD enzyme is a DNA helicase with fast and slow motors of opposite polarity

Andrew F. Taylor & Gerald R. Smith

Fred Hutchinson Cancer Research Center, Seattle, Washington 98109-1024, USA

Helicases are molecular motors that move along and unwind double-stranded nucleic acids[1]. RecBCD enzyme is a complex helicase and nuclease, essential for the major pathway of homologous recombination and DNA repair in *Escherichia coli*[2]. It has sets of helicase motifs[1] in both RecB and RecD, two of its three subunits. This rapid, highly processive enzyme unwinds DNA in an unusual manner: the 5′-ended strand forms a long single-stranded tail, whereas the 3′-ended strand forms an ever-growing single-stranded loop and short single-stranded tail. Here we show by electron microscopy of individual molecules that RecD is a fast helicase acting on the 5′-ended strand and RecB is a slow helicase acting on the 3′-ended strand on which the single-stranded loop accumulates. Mutational inactivation of the helicase domain in RecB or in RecD, or removal of the RecD subunit, altered the rates of unwinding or the types of structure produced, or both. This dual-helicase mechanism explains how the looped recombination intermediates are generated and may serve as a general model for highly processive travelling machines with two active motors, such as other helicases and kinesins.

Most helicases form Y-shaped molecules, with two equal-length single-stranded tails, during the unwinding of duplex DNA, but RecBCD enzyme forms structures with a single-stranded loop and two single-stranded tails. This unusual topology was demonstrated by electron microscopy of reaction intermediates[3], as shown in Fig. 1a. Both the extent of unwinding and the size of the loop increase linearly with time for tens of kilobases, at rates of ~370 and ~150 nucleotides s^{-1}, respectively[3] (see also Fig. 3a). The ever-